Molecular Organization of Amyloid Protofilament-Like Assembly of Betabellin 15D: Helical Array of β-Sandwiches

Hideyo Inouye,* Jeremy E. Bond,* Sean P. Deverin,* Amareth Lim,† Catherine E. Costello,† and Daniel A. Kirschner*

*Biology Department, Boston College, Chestnut Hill, Massachusetts 02467-3811 and †Department of Biochemistry, Boston University School of Medicine, Boston, Massachusetts 02118-2526 USA

ABSTRACT Betabellin is a 32-residue peptide engineered to fold into a four-stranded antiparallel β-sheet protein. Upon air oxidation, the betabellin peptides can fold and assemble into a disulfide-bridged homodimer, or β-sandwich, of 64 residues. Recent biophysical and ultrastructural studies indicate that betabellin 15D (B15D) (a homodimer of HSLTAKI**pk**LTFSIA**ph**TYTCAV**pk**YTAKVSH, where **p** = DPro, **k** = DLys, and **h** = DHis) forms unbranched, 35-Å wide assemblies that resemble the protofilaments of amyloid fibers. In the present study, we have analyzed in detail the X-ray diffraction patterns of B15D prepared from acetonitrile. The fiber diffraction analysis indicated that the B15D fibril was composed of a double helix defined by the selection rule $l = n + 7m$ (where l is even, and n and m are any integers), and having a 199-Å period and pitch, 28-Å rise per unit, and 10-Å radius. This helical model is equivalent to a reverse-handed, single helix with half the period and defined by the selection rule $l = -3n + 7m$ (where l is any integer). The asymmetric unit is the single B15D β-sandwich molecule. These results suggest that the betabellin assembly that models the protofilaments of amyloid fibers is made up of discrete subunits on a helical array. Multiple intersheet hydrogen bonds in the axial direction and intersandwich polar interactions in the lateral direction stabilize the array.

INTRODUCTION

Betabellins (beta-sandwich bell-shaped proteins) are a series of proteins designed de novo to explore the basic principles of protein folding (Richardson and Richardson, 1989). Betabellin 15S (B15S) is a 32-residue polypeptide chain having the sequence HSLTAKI**pk**LTFSIA**ph**TYTCAV**pk**YTAKVSH (where **p** = DPro, **k** = DLys, **h** = DHis) in which the D-amino acid residues have been strategically positioned to favor formation of type-I′ β turns (Yan et al., 1993, 1995). Air oxidation of B15S yields a 64-residue, disulfide-bridged, two-chain molecule betabellin designated 15D (B15D) (Lim et al., 1998, 1999). In 5.0 mM 3-(*N*-morpholino)propanesulfonate and 250 mM NaCl at pH 7, B15D forms a 35-Å wide fibrillar structure (Lim et al., 1998, 2000) that is unbranched and resembles the protofilaments of amyloid fibrils (Shirahama and Cohen, 1967; Fraser et al., 1991). The B15D assemblies bind Congo red and display an apple-green birefringence (Lim et al., 2000). X-ray diffraction patterns of B15D samples dried from aqueous solution give a strong meridional reflection at 4.7 Å and a broad equatorial reflection at ~10 Å, indicating that the β strands are oriented nearly perpendicular to the fibril axis (Lim et al., 2000). The B15D fibrillar structure has been proposed as a candidate for deriving a detailed molecular model of amyloid fibril assemblies (Lim et al., 2000).

X-ray diffraction has been used to study structure and assembly of a variety of amyloid fibers. These include the fibrils associated with neurological diseases, i.e., Alzheimer's β-amyloid protein (Fraser et al., 1992; Inouye et al., 1993; Malinchik et al., 1998), and prions (Nguyen et al., 1995; Inouye and Kirschner, 1997, 1998; Inouye et al., 2000), and with Familial amyloidotic polyneuropathy (FAP) (Blake and Serpell, 1996; Inouye et al., 1998). All diffraction patterns show wide-angle reflections that can be interpreted as arising from β-crystallites with the hydrogen-bonding direction running along the fiber axis. With the β-chains running normal or approximately normal to the fiber direction, the fibril is formed by the β-chains in a "cross-β" arrangement. Aβ(1–40) and Aβ(9–29) give small-angle meridional reflections that suggest a 50–70-Å periodicity along the H-bonding direction (Inouye et al., 1993), and FAP fibrils give successive wide-angle meridional reflections that indicate a longer periodicity along the fiber (Blake and Serpell, 1996; Inouye et al., 1998). Because the constituent transthyretin (TTR) molecule in the FAP fibril contains β-chains, the longer period can arise from the stacking of TTR monomers with the H-bonding between the β-chains aligned along the fiber direction (Inouye et al., 1998).

In the present study, we show for the first time the low-angle layer lines that are characteristic of the helical array from the B15D assemblies dried from acetonitrile (ACN). Analysis of these X-ray patterns indicated that the B15D molecules are arranged as a double helical array defined by the selection rule $l = n + 7m$ (where l is even, and n and m are any integers), and having a 199-Å period

---

Submitted January 7, 2002, and accepted for publication April 29, 2002.

Address reprint requests to H. Inouye and D. A. Kirschner, Biology Department, Higgins Hall 510, Boston College, 140 Commonwealth Ave., Chestnut Hill, MA 02467-3811. Tel.: 617-552-0211; Fax: 617-552-2011; E-mail: inouyeh@bc.edu and kirschnd@bc.edu.

Dr. Bond's current address is Global Prior Art, Inc., 21 Milk St., Boston, MA 02109.

0006-3495/02/09/1716/12 $2.00

and pitch, 28-Å rise per unit, and 10-Å radius. This helical array is equivalent to a reverse-handed, single helix with half the period and the selection rule $l = -3n + 7m$ (where l is any integer). The asymmetric unit is the single B15D β-sandwich molecule. The overall molecular organization of betabellin that models an amyloid protofilament thus consists of a double helical array of β-sandwich molecules.

MATERIALS AND METHODS

Engineering of B15D

The de novo design, solid phase synthesis, purity, and biophysical characterization of B15D has been described previously (Lim et al., 1998, 1999). The stock solutions were 250 μM B15D (~1.7 mg/mL), 50 mM 3-(*N*-morpholino)propanesulfonate at pH 7 (Sigma Chemical Co., St. Louis, MO), and 2.0 M NaCl (Fisher Scientific, Pittsburgh, PA). These solutions were prepared using the in-house reverse osmosis-purified water, which was further purified by passage through a Hydro Picotech 2 water purification system (Research Triangle Park, NC). All solutions were then filtered through Millipore Ultrafree-MC 0.22-μm centrifugal filters (Bedford, MA).

Previous model of B15D

A previous molecular model of the B15D fibril (Lim et al., 1998) has fibril dimensions that are consistent with those determined by electron microscopy (Lim et al., 1998, 2000), and shows a cross-β arrangement of the β-strands, which is consistent with the X-ray diffraction patterns (Lim et al., 2000). Secondary structure algorithms (DSSP by Kabsch and Sander, 1983; and STRIDE by Frishman and Argos, 1995) predict the same secondary structure mapping shown by the molecular model—i.e., four extended β strands (*e*) interspersed by three β turns (**t**):

HSLTAKI**pk**LTFSIA**ph**TYTCAV**pk**YTAKVSH
eeeeee**tt**eeeeee**tt**eeeeee**tt**eeeeee

The model proposes that the β strands in the one-dimensional stacking of the B15D molecules are tilted by ±15° from the direction perpendicular to the fibril axis (Lim et al., 1998). The asymmetric unit in the assembly is the individual B15D molecule. In the present study, we have used the atomic coordinates from this molecular model of the B15D molecule as the asymmetric unit in the helical array. The physicochemical characteristics of the sequence were analyzed by methods involving Fourier transform and averaging (Inouye and Kirschner, 1991).

X-ray diffraction of B15D

A lyophilized B15D sample was dissolved in 50% ACN, resulting in a 10–15 mg/mL solution. This solution was filtered, vortexed to ensure complete mixing, and centrifuged at 16,000 × *g* for 20 min. The supernatant was then slowly drawn into siliconized, thin-walled glass capillary tubes (0.7-mm outer diameter; Charles A. Supper, Co., South Natick, MA). The tubes were sealed at one end and placed in a 2-Tesla permanent magnet (Charles A. Supper, Co.; Oldenbourg and Phillips, 1986). The solvent was then allowed to evaporate slowly under ambient conditions. When the solutions had dried to small, uniform disks, the capillary tubes were removed from the magnetic field and transferred to an x-ray diffraction sample holder.

X-ray diffraction patterns were obtained by using nickel-filtered, double-mirror focused CuKα radiation from an Elliott GX-20 rotating anode x-ray generator (GEC Avionics, Hertfordshire, U.K.) operated at 35 kV and 35 mA. The patterns were recorded on Kodak DEF film (Rochester, NY) with exposure times of 100–121 h (Fig. 1 and Table 1). The known Bragg spacing of calcite (3.035 Å) was used to calibrate the specimen-to-film distance (74.0 and 86.0 mm). The diffraction patterns were digitized at 50-μm resolution using a personal SI densitometer (Molecular Dynamics, Sunnyvale, CA). The machine readout (in optical density units, OD) was calibrated internally and confirmed to be linear from 0 to 3 OD using the known optical density of a Kodak Step Calibration Tablet (No. 2; range from 0.04 to 3.03 OD). The digitized image was displayed on NIH IMAGE (developed at the U.S. National Institutes of Health and available at http://rsb.info.nih.gov/nih-image/). The intensities along layer lines and meridional and equatorial directions were plotted by selecting narrow windows. The background curves were approximated as polynomials and subtracted from the measured intensity data (Inouye et al., 1989). On the equator, Bragg reflections arising from the hexagonal lattice and the intersheet reflection at ~10 Å were observed. Each reflection was assumed to be a Gaussian function. Measurements of the integral widths and integral intensities of the reflections were obtained by fitting the background corrected intensity profile to multiple Gaussian functions. The actual fit to the observed intensity curve was carried out by optimizing the input data (i.e., the peak height and half width) using a least-square procedure (Inouye et al., 1989). The integral width B of the direct beam, determined after Gaussian approximation, was 1.86×10^{-3} Å^{-1} − 2.60×10^{-3} Å^{-1}.

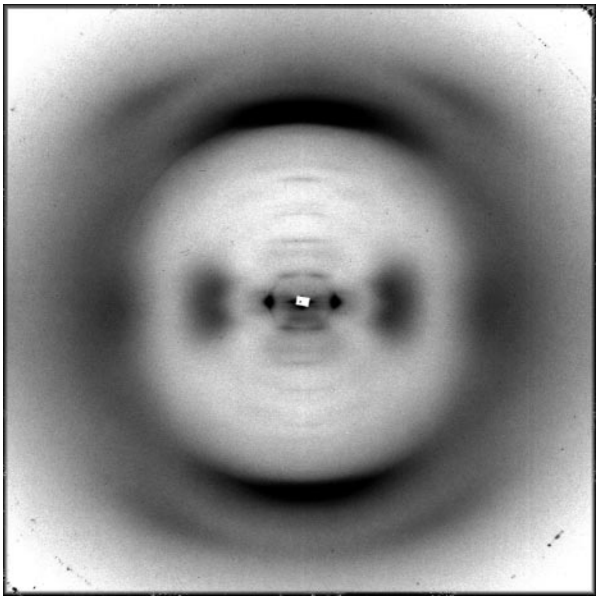

FIGURE 1 X-ray diffraction of B15D (dried from 50% ACN) with the incident beam perpendicular to the fibril axis (*vertical*). The exposure time was 121 h, and the specimen-to-film distance was 86.0 mm. The spacings are shown in Table 1 (column A) and Table 2 (column 3). The original pattern was densitometer-traced using a 50-μm raster. The image presented here has been contrast-enhanced for clarity.

For a discrete helix—i.e., one having a finite number of lattice points N, rise per unit h, and disorder parameter $\beta = \exp(-n^2 \langle\delta^2\rangle/2 - 2\pi^2 Z^2 \langle\Delta^2\rangle)$, where n is the Bessel order of J_n, δ and Δ are random angular and translational disorders at axial coordinate Z (as measured by the standard deviation of a Gaussian function)—paracrystalline theory indicates that the observed integral width squared for an x-ray reflection is given by $w_{\mathrm{obs}}^2 = B^2 + 1/(Nh)^2 + [(1 - \beta)/2h]^2$, where $1/(Nh)$ is the integral width of the coherent length for a perfect lattice (Inouye, 1994; Appendix). The disorder parameters were derived from the known observed integral widths of the direct beam and the layer line along the fibril direction.

The fibril tilt angle β was calculated according to $\tan(\beta) = (v_1 + v_2)(1 - \lambda^2 D^2/2)/(s\lambda^2 D^2)$, where v_1 and v_2 are the corresponding v-axis film

TABLE 1 Observed Bragg spacings (Å) for B15D diffraction patterns

Sample A	Sample B	Sample C
24.8 (*E* vs)	30.9 (*E* w) (11)	47.7 (*E* m) (01)
9.08 (*E′* s)	15.9 (*E* m) (22)	28.1 (*E* m) (11)
4.80 (*E* w)	11.4 (*E′* m)	16.1 (*E* vw) (03)
	5.00 (*E* w)	10.4 (*E′* m)
88.4 (*M′* w) 2	33.2 (*M* vw)	33.2 (*M* w)
44.2 (*M′* s) 4	23.9 (*M* vw)	24.1 (*M* vw)
33.2 (*M′* m) 6	18.0 (*M* w)	16.8 (*M* vw)
17.7 (*M′* vw) 12	14.0 (*M* w)	14.4 (*M* w)
14.0 (*M* w) 14	9.94 (*M* w)	9.18 (*M* vw)
9.91 (*M* w) 20	8.94 (*M* w)	7.10 (*M* w)
8.79 (*M* vw) 22	7.10 (*M* w)	6.60 (*M′* w)
7.69 (*M′* vw) 26	6.45 (*M* w)	4.98 (*M′* m)
7.10 (*M* w) 28	4.91 (*M* w)	4.72 (*M* vs)
6.44 (*M′* vw) 30	4.72 (*M* vs)	4.12 (*M* w)
5.17 (*M* vw) 38	4.09 (*M* vw)	3.60 (*M′*)
4.91 (*M′* w) 40	3.71 (*M′*)	
4.76 (*M* vs) 42		
4.12 (*M* vw) 48		
3.67 (*M′*)		

Three B15D samples dried from ACN solution gave well oriented diffraction patterns showing many layer lines. Variations in spacings for different samples are likely due to different hydration. The equatorial reflections were indexed by hexagonal lattices (Table 2). The intensities are qualitatively indicated by vs, very strong; s, strong; m, medium; w, weak; and vw, very weak.

Reflections that were clearly off-meridional are indicated by *M′*, otherwise by *M*. *E*, equator; *E′*, off-equator.

Sample A, whose pattern is shown in Fig. 1, is so well-oriented that some reflections are clearly off-meridional. However, most of the reflections on layer lines were labeled *M* owing to disorientation, as in Samples B and C. The ~10-Å equatorial, ~4.7-Å meridional, and ~3.7-Å off-meridional reflections are characteristic of cross-β sheets in an orthogonal lattice. When Sample C was oriented with its hydrogen-bonding direction parallel to the incident x-ray beam, 2D reflections at 48.2 Å (*E* s) (10) and 26.6 Å (*E′* m) (11) of 54.4-Å unit cell hexagonal lattice were observed. The fibril tilt angle was 7.7° for Sample A and 3.5° for Sample B. A stronger 4.7-Å reflection indicates a greater amount of fibril tilting owing to intersection with the Ewald sphere. The coherent domain size in the fibril direction of Sample A was ~160 Å from the integral widths (Gaussian distribution) of the strictly meridional reflections at 14 Å and 7 Å, assuming there was no lattice disorder. In the presence of translational disorder (Inouye, 1994), the domain size should become larger than the 199-Å fibril period. The minimum estimate of the domain size along the equatorial direction was 25 Å based on the width of the ~10-Å intersheet reflection. This size is similar to that for the two β sheets of the B15D molecule (Lim et al., 1998).

coordinates (vertical direction) for the reciprocal points (R, Z) and $(R, -Z)$, λ is the x-ray wavelength, D is the amplitude of a position vector in reciprocal space, which is the inverse of the observed Bragg spacing, and s is the specimen-to-film distance (Inouye et al., 1993). A positive tilt angle β corresponds to the fibril axis tilted away from the Ewald sphere. The v coordinate is written in terms of the u coordinate (horizontal direction) as $v^2 = t^2 - u^2$, where t is the distance of the reflection from the origin of the film (the position at which the incident beam impinges on the flat film) and is given by $t = s \tan\{2[a \sin(D\lambda/2)]\}$. The tilt angle was measured as $-7.7°$ and $-3.5°$ from two highly oriented fibril patterns (Table 1, Samples A and B). Note that tilting the fibril toward the Ewald sphere gives a stronger meridional 4.7-Å reflection. This tilt angle was taken as an average; and its variation was not measured. In this study, we assumed that the reciprocal coordinates were fully mapped on the film coordinates due to variations of fibril tilt angle and that the broadening of the reflections due to fibril disorientation was within the area of the narrow windows selected on the NIH Image display.

Molecular modeling

Molecular models were displayed and manipulated using MOLSCRIPT (Kraulis, 1991), XtalView (McRee, 1992), and Swiss-PDB Viewer (Guex and Peitsch, 1997; Guex et al., 1999). The secondary structure was determined from the atomic coordinates with DSSP (Kabsch and Sander, 1983) and STRIDE (Frishman and Argos, 1995; http://www.embl-heidelberg.de/stride/stride_info.html). The MOLSCRIPT representation was based on the assigned α helix and β strand. The number density of the amino acids was calculated as a function of distance from the center of mass. The size and the projection of the molecule were calculated from the atomic coordinates as previously described (Inouye et al., 1998).

RESULTS

Characteristic cross-β reflections

Three diffraction patterns of B15D dried from ACN (Fig. 1, Table 1) were analyzed. The fibril axis was in the meridional direction and was assigned as a cylindrical axis. All patterns showed a strong and intense 4.7-Å meridional reflection, a 3.7-Å off-meridional reflection, and an ~10-Å broad equatorial reflection. These reflections are indicative of a cross-β conformation (Geddes et al., 1968; Inouye et al., 1993). The fibril axis was approximately in the direction of hydrogen bonding. The above reflections were indexed as (200), (210), and (001) of an orthogonal unit cell having dimensions $a = 9.4$ Å, $b = 6.6$ Å, and $c = 10$ Å, where the a, b, and c axes correspond to the hydrogen bonding, chain, and intersheet directions (Fig. 1, Table 1). Small variations in Bragg spacings of these reflections (Table 1) likely arise from different hydration in the samples.

Equatorial reflections

Low-angle equatorial reflections varied for the different samples although they all had been prepared in the same way by drying from 50% ACN (Table 2 and Fig. 2). There were three distinctly different types of equatorial low-angle reflections: 1) two reflections at 43–48 and 24–28 Å (Table 2, Samples 1 and 2); 2) a single reflection at 25 Å (Table 2, Samples 3 and 4); and 3) two reflections at 31–39 and 16–18 Å (Table 2, Samples 5 and 6). The reflections were indexed by a two-dimensional hexagonal lattice having a unit cell of 49–56 Å (type 1) or 62–78 Å (type 3) (Table 2). The intensity of the (01) reflection was always less than that of the (11). The positions of these intensity minima at 0.031 and 0.051 $Å^{-1}$ corresponded to the first and second zeroes of the Fourier transform for either a tubular or solid cylinder. Our calculations revealed that the relative error between the observed and calculated intensity was smaller for a tubular versus solid cylinder, thus favoring the former as a better approximation to the fibril structure at low resolution.

TABLE 2 Summary of equatorial spacings

	Sample					
	1	2(C)	3(A)	4	5(B)	6
Spacing (Å)	43.0 (01) 24.3 (11)	47.7 (01) 28.1 (11) 16.1 (03)	24.8	25.3	30.9 (11) 15.9 (22)	38.7 (11) 17.5 (04)
Intersheet (Å)	9.26	10.4	9.08	9.32	11.4	11.2
Angular split (°)		20	20		15	
r_t (Å)	15	15			19	24
a (Å)	49.2	55.6			61.7	77.5
R	0.04	0.26			0.35	0.27

The equatorial spacings (Å) are summarized for different samples prepared by drying from ACN solution. Samples 3, 5, and 2, respectively, are the same as A, B, and C of Table 1. The diffraction pattern for Sample 3(A) is shown in Fig. 1. The difference in spacing among the samples is likely due to different hydration. The two-dimensional indices of the hexagonal lattice (lattice constant a) are shown in the parentheses. Because the intensity maximum of the intersheet reflection was off-equatorial, the angular split between the two reflections across the equator was measured on the enhanced diffraction patterns using NIH Image. The tubular radius r_t was derived from the expected intensity minima or maxima and used as an initial phase model. The agreement between the observed and phase model was evaluated by the relative residual between the observed and calculated structure amplitudes ($R_{\text{amp-obs}}$). The intersheet spacing clearly decreases with the decrease in the lattice constant. The angular split appears to be larger for the smaller intersheet spacing.

The radius of the tubular structure was measured as 15–24 Å (Table 2), which is consistent with the measured radius of B15D fibrils from electron microscopy (Lim et al., 2000). The calculated electron density maps projected along the fibril direction (Fig. 2, *insets*) showed looser packing of the tubular fibril assemblies in samples having larger hexagonal unit cells.

The intersheet separation varied such that larger values correlated to larger tubes that were arrayed in larger hexagonal lattices. For example, the 11-Å intersheet spacing was observed for the samples having lattice constants of 61.7 and 77.5 Å. A smaller intersheet separation of 9 Å was observed for the 49-Å lattice. A broad equatorial reflection at ~10 Å, which covered the layer lines $l = 0-6$, was not strictly on the equator. The angle between the intensity maximum and the equator ("angular split" in Table 2) suggested that the intersheet direction in the β sheet was more tilted from the direction perpendicular to the fibril axis for the smaller than for the larger lattice—e.g., 20° for $a = 55.6$ Å versus 15° for $a = 61.7$ Å. These observations may indicate that the two β sheets are offset or slide past one another in the fibril direction and are tilted more as the lattice unit cell decreases.

Layer lines

The diffraction pattern contained many layer lines with near-meridional reflections (Fig. 1 and Table 1). These reflections were interpreted as arising from a discrete helical array described by the selection rule $l = n + 7m$, where n and m are integers. The fibril period c and pitch P are 199 Å, and the rise per unit (h) is 28 Å. As a result, the strong meridional reflection at 4.76 Å was indexed as $l = 42$, $n = 0$, and $m = 6$ (Table 3). Because the odd order layers were not clearly defined, they were indexed as even orders, and the selection rule was written alternatively as $l = 2l' = n + 7m$, with $c = 199$ Å; $h = 28$ Å; l', n, and m are any integers; and l is an even integer. This expression can be denoted equivalently as $l' = 4n + 7m$ in the same sense and $l' = -3n + 7m$ in the opposite sense with $c = 199/2$ Å and $h = 28/2$ Å. The absence of odd orders in the helical lattice of period $c = 199$ Å was interpreted as arising from parallel double helices in the former or a generic single helix in the latter (Appendix). In the following description, the layer line number is indicated by l, and the period c is 199 Å.

The helix radius r_h refers to the position of the center of mass from the axis of the helix for the asymmetric unit. The average value 10.2 Å that was obtained for the radius was estimated from the peak position on the selected layer lines of 88, 44, 33, and 4.91 Å ($l = 2$, 4, 6, and 40) corresponding to J_2, J_4, J_{-1}, and J_{-2} intensity maxima ($x_{\max} = 2\pi r_h R$, where $1/R$ is the Bragg spacing along the radial direction), i.e., 3.1, 5.4, 1.8, and 3.1 Å (Table 4).

Given 0.74 cm^3/g as the specific volume for proteins (Matthews, 1968), 7022 Da as the molecular mass for B15D (Lim et al., 1998), and 124,375 Å^3 as the volume of the unit cell (25 Å × 25 Å × 199 Å, where 2 Å is from the equatorial reflection (Table 1, Sample A) and 199 Å is the periodicity along the fibril axis), we calculated that there were 14 B15D molecules within the unit cell. Because a single helix consists of 7 units per axial period, this number closely agrees with the 14 molecules for the double helix.

Model calculations

The molecular model of the asymmetric unit on a helical array was built and then was tested against the low-angle region of the observed intensities near the meridional axis in the range of radial coordinates up to 0.07 Å^{-1} on layer lines $l = 2$, 6, 14, and 28 (Table 3). The equatorial intensity and the higher layer lines were not used for comparison with the calculated intensity, because the interference between fibrils

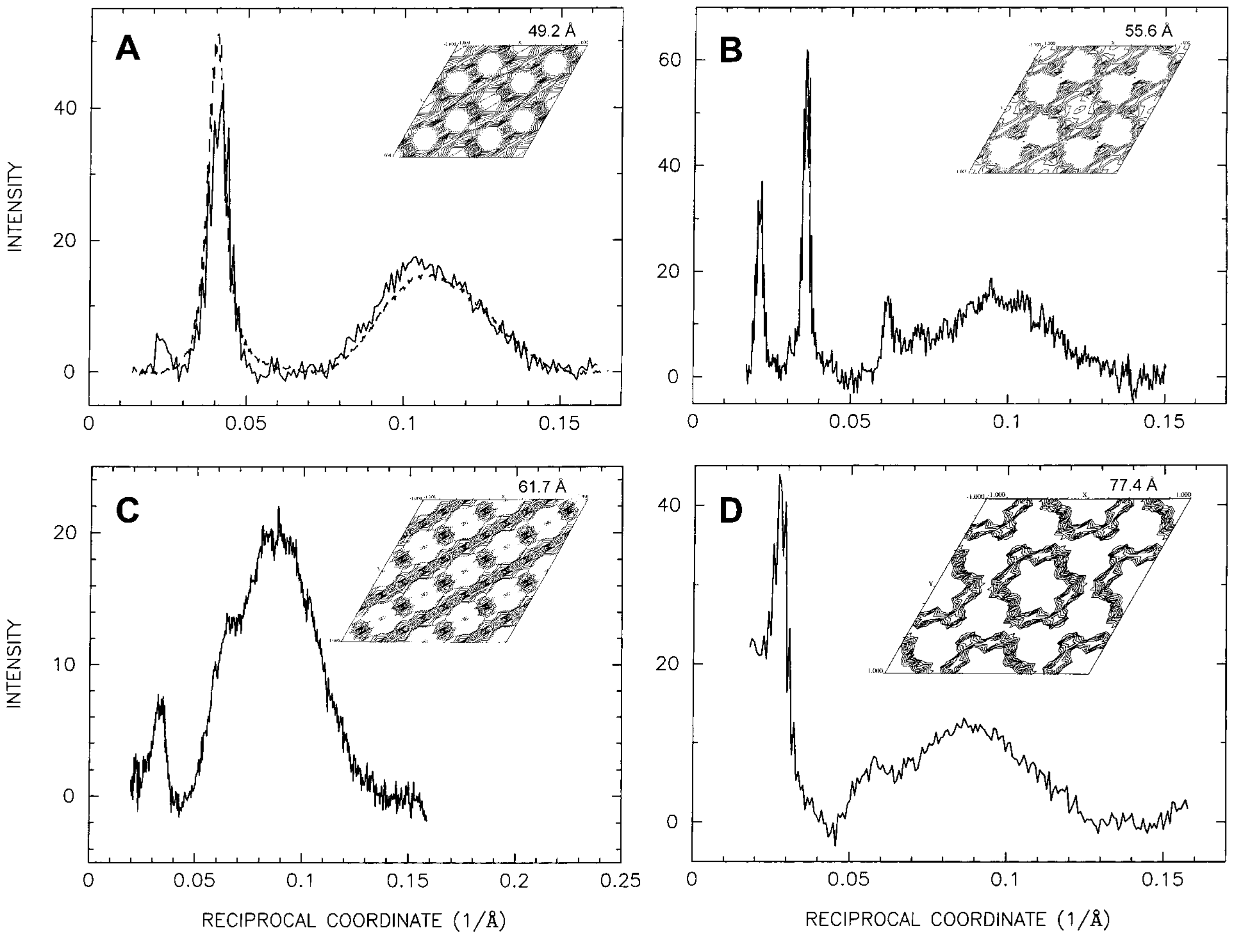

FIGURE 2 Observed equatorial intensities (normalized) as a function of radial coordinate (1/Å) for the different samples. The reflections are shown in Table 2. The unit cell constant for the hexagonal lattice is *a*. (*A*) Sample 1 (*solid line*) $a = 49.2$ Å and Sample 3 (*dashed line*). (*B*) Sample 2, $a = 55.6$ Å. (*C*) Sample 5, $a = 61.7$ Å. (*D*) Sample 6, $a = 77.4$ Å. *Insets*: The XtalView output of the electron density projection along the fibril direction as derived from the observed equatorial reflections and the phases of the tubular model. The intensities of the Bragg reflections arising from the hexagonal lattice and the intersheet reflection at ~10 Å were measured from the multiple Gaussian curves, which, after background subtraction, fit the observed total intensity to ~0.15 $Å^{-1}$. The circular tube-like electron density likely corresponds to the B15D fibril. When the hexagonal lattice constant increases, the size of the fibril increases.

is dominant on the equator, and it is experimentally very difficult to distinguish between meridional and nonmeridional diffraction on the higher layer lines.

A three-dimensional molecular model for B15D has been proposed (Lim et al., 1998). Secondary structure mapping by DSSP and STRIDE showed that the extended β-strands and β-turns alternate in the structure (see Materials and Methods, Previous model of B15D). The size of a B15D molecule was measured as 22 Å × 36 Å × 28 Å along the *x*, *y*, and *z* axes. The size in the *z* direction is similar to the rise per unit *h* for the helix defined by $l = n + 7m$, and *y* is similar to the fibril size (35 Å) as observed by electron microscopy (Lim et al., 1998, 2000). These similarities in size suggest that the B15D monomer is likely an asymmetric unit on a helical array. The previous model (Model 1) indicates that four β-chains form one β-sheet, and two parallel β-sheets constitute the periodic unit of the fiber. The two β-sheets are tilted from the fiber direction. Two other similar but variant models were also considered. These were constructed manually using molecular graphics programs (see Materials and Methods). For one (Model 2), the B15D molecule was tilted so that the H-bonding of one of the two β-sheets per molecule was aligned parallel to the fiber axis (Fig. 3). For the other (Model 3), the H-bonding directions of both β-sheets were put parallel to the fiber axis, resulting in a structural unit different from that in Models 1 and 2.

The cylindrically averaged intensity on the layer lines was calculated from the atomic coordinates of the three different models for an asymmetric unit according to the equation cited for a parallel double helix (Appendix) (Fig. 3). The values chosen were: helical radius = 10 Å, fibril period $c = \mathrm{P} = 199$ Å, and rise per unit $h = 28$ Å as derived from the x-ray diffraction data (Table 3 and 4). The second helix in relation to the first one was given by $\phi_{\mathrm{D}} = 0$ and $z_{\mathrm{D}} = 199$ Å/2 (see Fig. 3 and Appendix).

TABLE 3 Layer line spacings

l	n	d_{obs}	d_{calc}
0	0		
1	1		199.0
2	2	88.4	99.5
3	3		66.3
4	4	44.2	49.7
5	−2		39.8
6	−1	33.2	33.2
12	−2	17.7	16.6
14	0	14.0	14.2
20	−1	9.91	9.95
22	1	8.79	9.04
26	−2	7.69	7.65
28	0	7.10	7.10
30	2	6.44	6.63
38	3	5.17	5.23
40	−2	4.91	4.97
42	0	4.76	4.73
48	−1	4.12	4.14

Spacing of the layer lines is (l/c), where l is layer line number defined by $l = n + 7m$ and c is the periodicity along the helical axis. Here, the periodicity is the same as pitch $c = P = 199$ Å, and the unit rise h is 28 Å. The relative error between the observed and calculated spacings was 6.4%.

The maximum $n_{max} = 2\pi\, r_h R_{max}$ Bessel term of J_n was as previously given (Inouye et al., 1993). For example, the n_{max} for the equatorial position was 15, given $l = 0$, $R_{max} = 0.25$ Å^{-1}, and $r_0 = 10$ Å. The Fourier–Bessel transform was calculated within the range $-15 < n < 15$, where n satisfies the selection rule $l = un + vm$. As expected from the theory of parallel double helices (Appendix), the odd-order layer lines were absent, consistent with the observations.

The R factor was defined to measure the agreement between the observed and calculated structure amplitudes according to

TABLE 4 Helix radius r_h measured from layer line data

Z-axis (Å)	Layer line	R-axis (Å)	J_n term	$x_{max} = 2\pi r_h R$	r_h (Å)
88.4	2	20.1	2	3.1	9.91
44.2	4	9.94	4	5.4	8.54
33.2	6	44.4	−1	1.8	12.7
4.91	40	19.7	−2	3.1	9.73

The layer lines are indicated by the Bragg spacing (Å) along the fibril direction (Z-axis) and layer line number. The intensity maximum along the radial direction (R-axis) is shown as a Bragg spacing (Å). It corresponds to the intensity maximum of the J_n term, as indicated by x_{max}. The helix radius is given by r_h (Å).

$$R = \sum_j \left| |F_{obs_j}| - |F_{calc_j}| \right| \Big/ \sum_j |F_{obs_j}| ,$$

where

$$\sum_j |F_{obs_j}|^2 = \sum_j |F_{calc_j}|^2.$$

Both observed and calculated intensities, i.e., the squared structure amplitudes, were sampled by 0.00125 Å^{-1}. The j in the equation refers to the discrete structure amplitude. The summation covers intensities over the radial coordinate at all the selected layer lines. Here the observed radial components in the cylindrical coordinates are in the range of 0.00125 and 0.07 every 0.00125 Å (1⁄800 Å). For each model (Model 1, 2, or 3), two sets of intensities were calculated—from the peptide backbone alone and from the molecular structure containing all atoms including side chains. The R factors for the structure containing all atoms for three models were larger than those for the peptide backbone (see the in-text table). Among the models that were studied here, the peptide backbone of Model 2 gave the best fit to the observed data (R factor = 41%; Fig. 4). The relatively large R factor appears to come from the noise level of the observed

FIGURE 3 MOLSCRIPT representation of the double helical B15D Model 2. (*Left*) Projection along the radial direction. The constituent single helices are shown in the left and right parts, and the double helix is shown at the center. For clarity, the individual helices are colored differently. (*Right*) Projection along the fibril direction from the double helical part that contains four B15D asymmetric units per single helix, and shown at ~×2 compared to the radial projection on the left. The helical array of B15D molecules presented here was constructed in the following manner. First, the Cartesian coordinates (x, y, z) of the B15D Model 2 were defined as described in the previous study (Lim et al., 1998). Second, the center of gravity of the B15D molecule (x_0, y_0, z_0) was determined. Third, the coordinates (x, y, z) were modified according to (x–$x_0 + r_h$, y–y_0, z–z_0), where r_h is the helical radius. Fourth, the Cartesian coordinates were translated to cylindrical coordinates (r, φ, z), where $r^2 = (x\text{–}x_0 + r_h)^2 + (y\text{–}y_0)^2$ and $\varphi = \text{acos}[(x\text{–}x_0 + r_h)/r_h]$. Fifth, a series of coordinates (r, $\varphi + 2\pi nh/P$, $z + nh$) was calculated by choosing sequential integer n. Finally, the cylindrical coordinates were converted back to Cartesian coordinates. The modeled fibrillar structure in the helical array was derived using the parameters $r_h = 10$ Å, $c = P = 199$ Å, and $h = 28$ Å. The size of the model was determined to be 40 Å, which is similar to the 35-Å fibril size measured from electron micrographs (Lim et al., 1998, 2000). The parallel double helical model was built by transferring the atomic coordinates by one-half period in the fibril direction (z-axis). The angular displacement ϕ_D was set to zero, and z_D was 199 Å/2 (refer to Appendix for nomenclature).

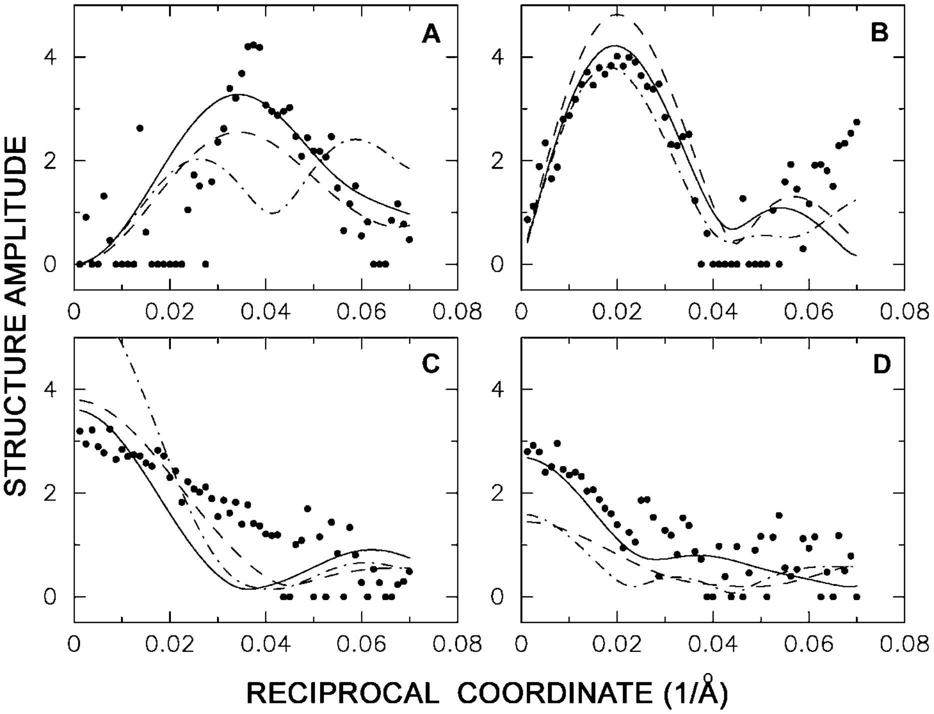

FIGURE 4 Comparison of the calculated (Model 1, *dashed line*; Model 2, *solid line*; Model 3, *dash-point-dash*) and observed (*filled circle*) amplitudes on selected layer lines *l*. (*A*) $l = 2$. (*B*) $l = 6$. (*C*) $l = 14$. and (*D*) $l = 28$. The curves were scaled so that the total intensities on these four layer lines became unity (see the definition of *R*-factor). The observed intensities were derived by extracting the image data within the narrow window on NIH image display and subtracting the polynomial-fit background. The calculated intensities of the near-meridional reflections show similar intensity maxima and minima as the observed reflections, indicating that the helix radius was correctly measured as 10 Å. The best fit was observed for the backbone structure of Model 2, which is shown in Figure 3.

intensity, because a Gaussian fit to the direct beam by itself gave an R factor as high as 27%.

	Model 1	Model 2	Model 3
Total structure	48%	48%	72%
Peptide backbone	45%	41%	58%

An antiparallel double helix was also studied by comparing the observed and calculated intensities (not shown); however, this model gave intensities for the odd-order layer lines, which were not seen in the observed diffraction pattern. Therefore, the parallel double helix is a better model for the B15D fibril.

DISCUSSION

Comparison with the transthyretin amyloid fibril

A continuous β-sheet helix, based on analysis of fiber diffraction from FAP fibrils, has been proposed as the universal molecular structure for amyloid fibrils (Blake and Serpell, 1996, Sunde et al., 1997). The selection rule of the helix in their model indicates $l = n + 24m$, $c = P = 115.5$ Å and $h = 4.8$ Å. Because the rise per unit h corresponds to the hydrogen bonding distance between β-strands, the helix is formed by continuous H-bonding in the fiber direction. The authors indexed some reflections as odd-order layer lines, but, according to helical theory (Klug et al., 1958; see Appendix), this is not actually valid for the double helical model. However, a structural perturbation may account for this.

Our analysis of the diffraction pattern of TTR fibrils from an FAP patient (Inouye et al., 1998) demonstrates that the fibrils are made up of an array of subunits, in which there is the 29-Å period stacking of four hydrogen-bonded β strands (as in the TTR monomeric subunit). Our current diffraction studies of the B15D assemblies suggest a similar model for the B15D fibrils, where the rise per unit $h = 28$ Å for a single helix. This similarity in dimensions most likely results from the similar molecular sizes of the B15D β-sandwich and the TTR structural unit, which both consist of a pair of four-stranded β sheets. Whether the subunits are arranged in a one-dimensional linear array as in the TTR fibrils or in a helical array as in the B15D fibrils may depend on the protein–protein interactions at the subunit interface.

Diagonal and translational interactions between asymmetric units

Interactions among subunits in the diagonal versus fibril (translational) direction are expected to result in different protein assemblies. For the double helix, one helix may not easily "slide" against the other in the axial direction if the diagonal interaction between side chains in the generic helix is strong. However, the helically arrayed asymmetric units may still deviate from their ideal positions due to angular disorder. When the translational interaction between asymmetric units in a single helix is strong, one helix may easily slide against the other. Diagonal and translational disorders between asymmetric units have been studied previously to explain the variable cross-over distance observed by electron microscopy for actin fibrils—e.g., a model of cumulative angular disorder (Egelman and DeRosier, 1982) and a model invoking lateral slipping between double helices (Censullo and Cheung, 1993). The scattering intensity for a generic helix having angular and translational disorders has been derived previously (Inouye, 1994).

Equations for helical diffraction that includes slipping between the helices were derived to analyze the diffraction patterns of B15D (Appendix). The consequence of the cumulative angular disorder is that the intensity of the layer lines having a higher order Bessel term decreases while the peak width in the fibril direction and the background intensity increase. Because the meridional and equatorial reflections are not influenced by these disorders, the observed reflections are largely restricted to meridional and equatorial axes, and wide-angle reflections are weak and broader in the fibril direction. Angular and translational disorders explain why the near-equatorial 10-Å reflection is not restricted on layer lines $l = 0-6$, and intensity fills the space between the layer lines. Analysis of perturbations in the relative movement (or slipping) within a double helix—e.g., where one helix shifts by half a period along the fibril direction relative to the other—predicts that the odd-order layer lines will be completely absent if there is no perturbation, but will show intensity when the relative positions of the two helices are perturbed (Appendix). Because the observed B15D diffraction pattern (Fig. 1 and Table 1) did not show strong odd-order layer lines (including $l = 7$, which corresponds to the J_0 Bessel term), any slipping perturbation is not significant for the B15D fibril.

Interaction among asymmetric units

The molecular model of B15D (Fig. 3) shows that, in the fibril direction, there are interactions between His-64 and Thr-27, and in the diagonal direction between Lys-61 and Lys-38 at the molecular interfaces of the B15D asymmetric units (Fig. 5). The space within the double helix contains positive-charge residues (Lys-38 and Lys-61). Because the diffraction pattern of B15D suggested that the diagonal interaction may be stronger than that in the fibril direction, the positive charges of the Lys residues are likely bridged by anions. Such anions may derive from the media at higher ionic strength because B15D does not fold at low ionic strength (Lim et al., 1998). The interaction in the fibril direction may occur via His-64 and Thr-27. If the His residue is protonated at acidic pH, the interaction will become weaker, consistent with the observation that protonation of one or more of the imidazole rings is sufficient to disrupt the β structure of B15D (Lim et al., 1998).

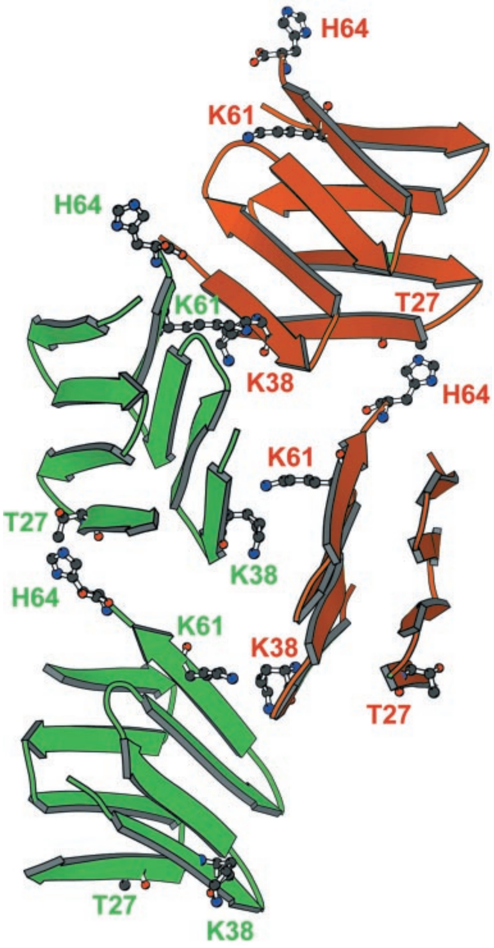

FIGURE 5 MOLSCRIPT representation of the interface between the two helices, showing ball and stick models of residues His-64 and Thr-27 in the fibril direction (*vertical*) and of Lys-38 and Lys-61 in the diagonal direction. Anions may counter the positive charges of these Lys residues (Lim et al., 1998). For clarity, the individual helices are colored differently, and the disulfide within each β-sandwich between Cys-21 and Cys-53 has been omitted.

Assembly of fibrils

Analysis of the equatorial x-ray reflections showed that the B15D fibrils assembled in a hexagonal lattice with period 49–77 Å. Electron microscopy also shows that the 35-Å wide protofilament assembles into a larger fibril (Lim et al., 1998). Because amyloid fibrils generally have diameters of ~100 Å and are constituted of 4–6 40-Å wide protofilaments (Inouye et al., 1993), it is important to investigate the inter-fibrillar interactions. Because α coiled-coil packing has been considered to be a common type of fibril assembly (Crick, 1953a,b; Pauling and Corey, 1953), the observed x-ray diffraction of B15D was analyzed to see whether it could be interpreted as arising from a coiled-coil structure (data not shown). As our calculation showed, coiled-coil packing may account for part of the meridional intensities, but the observed pattern seems to be predominantly accounted for by a double helix having no significant slipping disorder, suggesting that the double helices pack in a nearly parallel arrangement. The underlying physicochemical basis of this type of packing may be similar to the one responsible for the surprising preponderance of parallel packing motifs of RNA molecules in crystals (Murthy and Rose, 2000).

SUMMARY

B15S is an engineered peptide containing four hydrogen-bonded β strands. Upon oxidation, two molecules of B15S form B15D, a disulfide-bonded β sandwich. B15D formed highly, oriented fibrils that gave cross-β helical fiber patterns. The selection rule ($l = n + 7m$) for a double helix and the equivalent rule $l = -3n + 7m$ for a generic single helix were determined for the B15D fibrils. The width of the B15D fibril is consistent with that observed by electron microscopy. The rise per unit was the same as that for the extent of four β strands in the hydrogen-bonding direction. From these considerations, we built a helical model and calculated its diffraction pattern. The similarity between the rise per unit in the B15D fibril and the stacking period in the TTR fibril (Inouye et al., 1998) is due to the similar molecular arrangements of B15D and TTR—both B15D and TTR have four hydrogen-bonded strands per β sheet. These results suggest that their corresponding amyloid fibrils are built from discrete subunits. The polymorphic nature of subunit (or β-crystallite) assembly, e.g., one-dimensional stacking versus helical array, may arise from a variation in intersubunit protein–protein interactions. The interactions between the subunits in the hydrogen-bonding direction along the fibril axis is stronger in the linear assembly than in the helical assembly.

APPENDIX

X-ray diffraction theory

The x-ray scattering intensity function for a discrete helix with cumulative and noncumulative angular and translational disorders has been previously described (Inouye, 1994). For cumulative disorder, the intensity function is given by

$$I(R, Z) = \sum_{n=-\infty}^{\infty} |J_n(2\pi r_0 R)|^2 \langle S(n, Z)\rangle,$$

and

$$\langle S(n, Z)\rangle = \mathrm{Re}\left[\frac{N(1+H)}{1-H}\right] - 2\,\mathrm{Re}\left[\frac{H - H^{N+1}}{(1-H)^2}\right],$$

where R refers to the radial component of the cylindrical reciprocal coordinates, Z refers to the axial component, P is the pitch of the helix, h is the rise per subunit, r_0 is the radius of the helix, and $\Delta\varphi = 2\pi h/P$ (angular twist per unit). β is the function of random angular disorder δ and translational disorder Δ (as defined by the standard deviation of Gaussian function) according to $\beta = \exp(-n^2\langle\delta^2\rangle/2 - 2\pi^2 Z^2\langle\Delta^2\rangle)$, where N is the number of lattice point, n is the Bessel order, $H = \beta\exp[i\Delta\varphi(PZ - n)]$, and Re refers to the real part of the function.

Inclusion of the atomic coordinates is necessary for calculating the helix intensity from the molecular model. Discrete helices with cumulative disorders (angular and translational) were considered. The cylindrical coordinates (r_k, φ_k, z_k) are defined by the first atomic position of atom type j on a helix k where $0 \leq j \leq N - 1$ and $0 \leq k \leq M - 1$. The cylindrically averaged intensity $I(R, Z)$ at reciprocal cylindrical coordinates (R, Z) with the atomic factor $f_k(R, \Phi, Z)$ is given by

$$I(R, Z) = \sum_{k}\sum_{k'} f_k(R, \Phi, Z) f_{k'}(R, \Phi, Z)$$

$$\sum_{n} J_n(2\pi r_k R) J_n(2\pi r_{k'} R) \exp[-in(\phi_k - \phi_{k'})$$

$$\times \exp[i2\pi Z(z_k - z_{k'})]\langle S(n, Z)\rangle,$$

where

$$\langle S(n, Z)\rangle = N + \sum_{j}\sum_{j'} \exp[i(j - j')\Delta\phi(PZ - n)]\beta^{|j-j'|},$$

and

$$\beta = \exp(-n^2\langle\delta^2\rangle/2 - 2\pi^2 Z^2\langle\Delta^2\rangle).$$

When the helical structure is very long (N very large) and the helical selection rule is satisfied, the intensity maximum is given by $\langle S(n, Z)\rangle = N(1 + \beta)/(1 - \beta)$.

If the disorder parameters are neglected, the helical intensity reduces to the one for the ideal helix (Cochran et al., 1952; Franklin and Klug, 1955),

$$\langle I(R, \Phi, l/c)\rangle_\Phi = \sum_{n} (A_n^2 + B_n^2),$$

where

$$A_n = \sum_{j} f_j J_n(2\pi r_j R)\cos[n(\pi/2 - \phi_j) + 2\pi l z_j/c],$$

$$B_n = \sum_{j} f_j J_n(2\pi r_j R)\sin[n(\pi/2 - \phi_j) + 2\pi l z_j/c].$$

Here, the structure factor is written as

$$F(R, \Phi, l/c) = \sum_{n} G_n \exp[in(\Phi + \pi/2)],$$

where

$$G_n(R) = \sum_{j} f_j J_n(2\pi r_j R)\exp\, i[n(-\phi_j) + 2\pi l z_j/c].$$

The layer line number l is related to the Bessel term n according to the helical selection rule $l = un + vm$, where all variables are integers. The atomic coordinate j refers to the atoms in the asymmetrical unit.

Coaxial double helix

The structure factor of a single discrete helix can be expanded to the second helix (Lotz et al., 1976). In parallel strands, each atom at coordinate (r_j, ϕ_j, z_j) corresponds to the atom of the other strand at (r_j, $\phi_j + \phi_D$, $z_j + z_D$). The G_n term in the structure factor equation (see above) is replaced by $G_{nl}^{Dp}(R) = G_{nl}(R)(1 + \exp i\Gamma)$, where $\Gamma = -n\phi_D + 2\pi l z_D/c$. Note that 1 +

exp $i\Gamma$ can also be written as 2 cos(Γ/2)exp i(Γ/2) (Lotz et al., 1976). Thus, the intensity is

$$I = \sum G_{\mathrm{nl}}^{\mathrm{Dp}} G_{\mathrm{nl}}^{\mathrm{Dp}*} = \sum 2(1 + \cos\Gamma)(A^2 + B^2),$$

where A and B are given above. The asterisk (*) refers to the conjugate.

For an antiparallel double helix where the corresponding atoms are at (r_{j}, ϕ_{j}, z_{j}) and at (r_{j}, $-(\phi_{\mathrm{j}} + \phi_{\mathrm{D}})$, $-(z_{\mathrm{j}} + z_{\mathrm{D}})$) (Lotz et al., 1976), the G_{nl} term is given by

$$\begin{aligned} G_{\mathrm{nl}}^{\mathrm{Da}} &= 2(\exp - i\Gamma/2) \\ &\quad \times \sum_{\mathrm{j}} f_{\mathrm{j}} J_{\mathrm{n}}(2\pi r_{\mathrm{j}} R)\cos(-n\phi_{\mathrm{j}} + 2\pi l z_{\mathrm{j}}/c + \Gamma/2). \end{aligned}$$

The cylindrically averaged intensity is

$$I = \sum_{\mathrm{n}} |G_{\mathrm{nl}}^{\mathrm{Da}}|^2.$$

The intensities on any layer line are present in the antiparallel assembly, but they can be absent in the parallel assembly when $1 + \cos\Gamma = 0$. For example, if the second helix in the parallel assembly is shifted in the axial direction by $c/2$, then $\phi_{\mathrm{D}} = 0$, $z_{\mathrm{D}} = c/2$, and $\Gamma = l\pi$. When the layer line number l is odd, $1 + \cos\Gamma = 0$ is satisfied, indicating that the intensities of the odd-order layer lines are absent.

Effect of perturbation to the cylindrically averaged intensity for a parallel double helix

The Clark–Muus type disorder (Clark and Muus, 1962; Tanaka and Naya, 1969) for the terms ϕ_ρ and z_ρ may be written in terms of the average values $\bar{\phi}_{\mathrm{D}}$ and $\bar{z}_{\mathrm{D}}$ as $\phi_{\mathrm{D}} = \bar{\phi}_{\mathrm{D}} + \phi_\rho$ for the angular effect and $z_{\mathrm{D}} = \bar{z}_{\mathrm{D}} + z_\rho$ for the translational effect. Assuming a zero mean Gaussian distribution for ϕ_ρ and z_ρ, where the standard deviations are δ_ϕ and δ_z, the statistical average of the function due to angular or axial perturbations, e.g., $\langle g(\phi_\rho)\rangle$ or $\langle g(z_\rho)\rangle$, can be expressed as

$$\langle g(\phi_\rho)\rangle = \int 1/(\sqrt{2\pi\delta_\phi^2})\exp(-\phi_\rho^2/2\delta_\phi^2)g(\phi_\rho)\,\mathrm{d}\phi_\rho$$

or

$$\langle g(z_\rho)\rangle = \int 1/(\sqrt{2\pi\delta_{\mathrm{z}}^2})\exp(-z_\rho^2/2\delta_{\mathrm{z}}^2)g(z_\rho)\,\mathrm{d}z_\rho.$$

The cylindrically averaged intensity for a perturbed parallel double helix $\langle G_{\mathrm{nl}}^{\mathrm{Dp}} G_{\mathrm{nl}}^{\mathrm{Dp}*}\rangle$ is derived in the following manner. From the intensity function given above, [$G_{\mathrm{nl}}^{\mathrm{Dp}} G_{\mathrm{nl}}^{\mathrm{Dp}*} = 2(1 + \cos\Gamma)(A^2 + B^2)$], the statistically averaged intensity can be written as $\langle G_{\mathrm{nl}}^{\mathrm{Dp}} G_{\mathrm{nl}}^{\mathrm{Dp}*}\rangle = 2(1 + \langle\cos\Gamma\rangle)(A^2 + B^2)$, where $\langle\cos\Gamma\rangle = \langle\cos[-n(\bar{\phi}_{\mathrm{D}} + \phi_\rho) + 2\pi l c^{-1}(\bar{z}_{\mathrm{D}} + z_\rho)]\rangle$. The term $\langle\cos\Gamma\rangle$ for three different cases of angular and translational disorders is given below whereas the $\langle GG^*\rangle$ term is indicated below in the Table. If angular and translational displacements are random, $\langle\cos\Gamma\rangle = 0$. Then $\langle G_{\mathrm{nl}}^{\mathrm{Dp}} G_{\mathrm{nl}}^{\mathrm{Dp}*}\rangle = 2(A^2 + B^2)$, indicating that the diffraction pattern becomes the same as that for a single helix.

1. Small angular displacement and no translational displacement, where ϕ_ρ is small, and $z_\rho = 0$. Then

   $$\langle\cos\Gamma\rangle = \langle\cos(\bar{\Gamma} - n\phi_\rho)\rangle,$$

   and

   $$\begin{aligned} &\langle\cos\Gamma\rangle \\ &= \int 1/(\sqrt{2\pi\delta_\phi^2})\exp(-\phi_\rho^2/2\delta_\phi^2)\cos(\bar{\Gamma} - n\phi_\rho)\,\mathrm{d}\phi_\rho \\ &= \cos\bar{\Gamma}\,\exp(-n^2\delta_\phi^2/2). \end{aligned}$$

2. Small translational displacement and no angular displacement, where z_ρ is small and $\phi_\rho = 0$. Then

   $$\langle\cos\Gamma\rangle = \langle\cos(\bar{\Gamma} - 2\pi l c^{-1} z_\rho)\rangle$$

   and

   $$\begin{aligned} &\langle\cos\Gamma\rangle \\ &= \int 1/(\sqrt{2\pi\delta_{\mathrm{z}}^2})\exp(-z_\rho^2/2\delta_{\mathrm{z}}^2)\cos(\bar{\Gamma} - 2\pi l c^{-1} z_\rho)\,\mathrm{d}z_\rho \\ &= \cos\bar{\Gamma}\,\exp(-2\pi^2 l^2 c^{-2}\delta_{\mathrm{z}}^2). \end{aligned}$$

3. Screw disorder, which is defined by the relation between angular and translational displacements according to $z_\rho = P\phi_\rho/2\pi$. Then

   $$\langle\cos\Gamma\rangle = \langle\cos[\bar{\Gamma} + (-n + lP/c)\phi_\rho]\rangle$$

   and

   $$\begin{aligned} &\langle\cos\Gamma\rangle \\ &= \int 1/(\sqrt{2\pi\delta_\phi^2})\exp(-\phi_\rho^2/2\delta_\phi^2)\cos[\bar{\Gamma} + (-n + lP/c)\phi_\rho]\,\mathrm{d}\phi_\rho \\ &= \cos\bar{\Gamma}\,\exp[-(-n + lP/c)^2\delta_\phi^2/2]. \end{aligned}$$

Effect of perturbation on the cylindrically averaged intensity for an antiparallel double helix

From the structure factor for an antiparallel double helix, given by

$$\begin{aligned} G_{\mathrm{nl}}^{\mathrm{Da}} &= 2(\exp - i\Gamma/2) \\ &\quad \times \sum_{\mathrm{j}} f_{\mathrm{j}} J_{\mathrm{n}}(2\pi r_{\mathrm{j}} R)\cos(-n\phi_{\mathrm{j}} + 2\pi l z_{\mathrm{j}}/c + \Gamma/2), \end{aligned}$$

the averaged intensity (including the contribution due to the Gaussian distribution of the displacement) can be expressed as

$$\begin{aligned} &\langle G_{\mathrm{nl}}^{\mathrm{Da}} G_{\mathrm{nl}}^{\mathrm{Da}*}\rangle \\ &= 4\sum_{\mathrm{j}} f_{\mathrm{j}}^2 J_{\mathrm{n}}^2(2\pi r_{\mathrm{j}} R)\left\langle\cos^2\left(-n\phi_{\mathrm{j}} + \frac{2\pi l z_{\mathrm{j}}}{c} + \frac{\bar{\Gamma} - n\phi_\rho}{2} + \frac{\pi l z_\rho}{c}\right)\right\rangle \\ &\quad + 4\sum_{\mathrm{j}}\sum_{\mathrm{k}} f_{\mathrm{j}} f_{\mathrm{k}} J_{\mathrm{n}}(2\pi r_{\mathrm{j}} R) J_{\mathrm{n}}(2\pi r_{\mathrm{k}} R) \\ &\quad \cdot \left\langle\cos\left(-n\phi_{\mathrm{j}} + \frac{2\pi l z_{\mathrm{j}}}{c} + \frac{\bar{\Gamma} - n\phi_\rho}{2} + \frac{\pi l z_\rho}{c}\right)\right. \\ &\quad \left.\cdot \cos\left(-n\phi_{\mathrm{k}} + \frac{2\pi l z_{\mathrm{k}}}{c} + \frac{\bar{\Gamma} - n\phi_\rho}{2} + \frac{\pi l z_\rho}{c}\right)\right\rangle. \end{aligned}$$

Three different cases are considered in the following Table. The averaged intensity ξ^2 was derived in a similar way as described above for the parallel double helix:

	Averaged intensity ξ^2
Small ϕ_ρ and $z_\rho = 0$	$(n^2\delta_\phi^2)/2$
Small z_ρ and $\phi_\rho = 0$	$2\pi^2 l^2 c^{-2}\delta_z^2$
Screw disorder $z_\rho = \phi_\rho P/2\pi$	$(-n + lPc^{-1})^2\delta_\phi^2/2$

For the parallel double helix, $\langle G_{\mathrm{nl}}^{\mathrm{Dp}} G_{\mathrm{nl}}^{\mathrm{Dp}*}\rangle = 2(1 + \cos\bar{\Gamma}\exp - \xi^2)(A^2 + B^2)$, whereas, for the antiparallel double helix,

$$\langle G_{\mathrm{nl}}^{\mathrm{Da}} G_{\mathrm{nl}}^{\mathrm{Da}*}\rangle$$

$$= 2\sum_{\mathrm{j}} f_{\mathrm{j}}^2 J_{\mathrm{n}}^2(2\pi r_{\mathrm{j}}R)\left[1 + \cos 2\left(-n\phi_{\mathrm{j}} + \frac{2\pi l z_{\mathrm{j}}}{c} + \frac{\bar{\Gamma}}{2}\right)\exp(-\xi^2)\right]$$

$$+ 2\sum_{\mathrm{j}}\sum_{\mathrm{k}} f_{\mathrm{j}} f_{\mathrm{k}} J_{\mathrm{n}}(2\pi r_{\mathrm{j}}R) J_{\mathrm{n}}(2\pi r_{\mathrm{k}}R)$$

$$\cdot\left\{\cos\left[-n(\phi_{\mathrm{j}} + \phi_{\mathrm{k}}) + \frac{2\pi l(z_{\mathrm{j}} + z_{\mathrm{k}})}{c} + \bar{\Gamma}\right]\exp(-\xi^2)\right.$$

$$\left. + \cos[-n(\phi_{\mathrm{j}} - \phi_{\mathrm{k}}) + 2\pi l c^{-1}(z_{\mathrm{j}} - z_{\mathrm{k}})]\right\}.$$

We thank an anonymous referee for critical and constructive comments on the model calculations.

This research was supported by an Alzheimer's Association/T.L.L. Temple Discovery Award (D.A.K.), the Alzheimer's Disease Research Program of the American Health Assistance Foundation (D.A.K.), institutional support from Boston College (D.A.K.), and grant P41-RR-10888 from the National Institutes of Health, National Center for Research Resources (C.E.C.).

REFERENCES

Blake, C., and L. Serpell. 1996. Synchrotron x-ray studies suggest that the core of the transthyretin amyloid fibril is a continuous β-sheet helix. *Structure.* 4:989–998.

Censullo, R., and H. C. Cheung. 1993. A rotational offset model for two-stranded F-actin. *J. Struct. Biol.* 110:75–83.

Clark, E. S., and L. T. Muus. 1962. The relationship between Bragg reflections and disorder in crystalline polymers. *Z. Kristallogr.* 117: 108–118.

Cochran, W., F. H. C. Crick, and V. Vand. 1952. The structure of synthetic polypeptides. I. The transform of atoms on a helix. *Acta Crystal.* 5:581–586.

Crick, F. H. C. 1953a. The Fourier transform of a coiled-coil. *Acta Crystal.* 6:685–689.

Crick, F. H. C. 1953b. The packing of α-helices: simple coiled-coils. *Acta Crystal.* 6:689–697.

Egelman, E. H., and D. J. DeRosier. 1982. The Fourier transform of actin and other helical systems with cumulative random angular disorder. *Acta Crystal.* A38:796–799.

Franklin, R. E., and A. Klug. 1955. The splitting of layer lines in x-ray fibre diagrams of helical structures: application to tobacco mosaic virus. *Acta Crystal.* 8:777–780.

Fraser, P. E., L. K. Duffy, M. B. O'Malley, J. Nguyen, H. Inouye, and D. A. Kirschner. 1991. Morphology and antibody recognition of synthetic β-amyloid peptides. *J. Neurosci. Res.* 28:474–485.

Fraser, P. E., J. T. Nguyen, H. Inouye, W. K. Surewicz, D. J. Selkoe, M. B. Podlisny, and D. A. Kirschner. 1992. Fibril formation by primate, rodent and Dutch-haemorrhagic analogues of Alzheimer amyloid β-protein. *Biochemistry.* 31:10716–10723.

Frishman, D., and P. Argos. 1995. Knowledge-based protein secondary structure assignment. *Proteins.* 23:566–579.

Geddes, A. J., K. D. Parker, E. D. T. Atkins, and E. Beighton. 1968. "Cross-β" conformation in proteins. *J. Mol. Biol.* 32:343–358.

Guex, N., and M. C. Peitsch. 1997. SWISS-MODEL and the Swiss-PdbViewer: an environment for comparative protein modeling. *Electrophoresis.* 18:2714–2723.

Guex, N., A. Diemand, and M. C. Peitsch. 1999. Protein modelling for all. *Trends Biochem. Sci.* 24:364–367.

Inouye, H. 1994. X-ray scattering from a discrete helix with cumulative angular and translational disorders. *Acta Crystal.* A50:644–646.

Inouye, H., J. Bond, M. A. Baldwin, H. L. Ball, S. B. Prusiner, and D. A. Kirschner. 2000. Structural changes in a hydrophobic domain of the prion protein induced by hydration and by Ala → Val and Pro → Leu substitutions. *J. Mol. Biol.* 300:1283–1296.

Inouye, H., F. S. Domingues, A. M. Damas, M. J. Saraiva, E. Lundgren, O. Sandgren, and D. A. Kirschner. 1998. Analysis of x-ray diffraction patterns from amyloid of biopsied vitreous humor and kidney of transthyretin (TTR) Met30 familial amyloidotic polyneuropathy (FAP) patients: axially arrayed TTR monomers constitute the protofilament. *Amyloid Int. J. Exp. Clin. Invest.* 5:163–174.

Inouye, H., P. E. Fraser, and D. A. Kirschner. 1993. Structure of β-crystallite assemblies formed by Alzheimer β-amyloid protein analogues: analysis by x-ray diffraction. *Biophys. J.* 64:502–519.

Inouye, H., J. Karthigasan, and D. A. Kirschner. 1989. Membrane structure in isolated and intact myelins. *Biophys. J.* 56:129–137.

Inouye, H., and D. A. Kirschner. 1991. Folding and function of the myelin proteins from primary sequence data. *J. Neurosci. Res.* 28:1–17.

Inouye, H., and D. A. Kirschner. 1997. X-ray diffraction analysis of scrapie prions: intermediate and folded structures in a peptide containing two putative α-helices. *J. Mol. Biol.* 268:375–389.

Inouye, H., and D. A. Kirschner. 1998. Polypeptide chain folding in the hydrophobic core of hamster scrapie prion: analysis by x-ray diffraction. *J. Struct. Biol.* 122:247–255.

Kabsch, W., and C. Sander. 1983. Dictionary of protein secondary structure: pattern recognition of hydrogen-bonded and geometrical features. *Biopolymers.* 22:2577–2637.

Klug, A., F. H. C. Crick, and H. W. Wyckoff. 1958. Diffraction by helical structures. *Acta Crystal.* 11:199–213.

Kraulis, P. J. 1991. MOLSCRIPT: a program to produce both detailed and schematic plots of protein structures. *J. Appl. Crystallogr.* 24:946–950.

Lim, A., M. J. Saderholm, A. M. Makhov, M. Kroll, Y. Yan, L. Perera, J. D. Griffith, and B. W. Erickson. 1998. Engineering of betabellin-15D: a 64 residue β sheet protein that forms long narrow multimeric fibrils. *Protein Sci.* 7:1545–1554.

Lim, A., P. A. Guy, A. M. Makhov, M. J. Saderholm, M. Kroll, Y. Yan, R. J. Anderegg, J. D. Griffith, and B. W. Erickson. 1999. Engineering of betabellin 15D: copper(II)-induced folding of a fibrillar β-sandwich protein. *Lett. Peptide Sci.* 6:3–14.

Lim, A., A. M. Makhov, J. Bond, H. Inouye, L. H. Connors, J. D. Griffith, B. W. Erickson, D. A. Kirschner, and C. E. Costello. 2000. Betabellins 15D and 16D, de novo designed β-sandwich proteins that have amyloidogenic properties. *J. Struct. Biol.* 130:363–370.

Lotz, B., F. Colonna-Cesari, F. Heitz, and G. Spach. 1976. A family of double helices of alternating poly(gamma-benzyl-D-L-glutamate), a stereochemical model for gramicidin A. *J. Mol. Biol.* 106:915–942.

Malinchik, S. B., H. Inouye, K. E. Szumowski, and D. A. Kirschner. 1998. Structural analysis of Alzheimer's β(1–40) amyloid: protofilament assembly of tubular fibrils. *Biophys. J.* 74:537–545.

Matthews, B. W. 1968. Solvent content of protein crystals. *J. Mol. Biol.* 33:491–497.

McRee, D. E. 1992. XtalView: a visual protein crystallographic software system for X11/Xview. *J. Mol. Graph.* 10:44–47.

Murthy, V. L., and G. D. Rose. 2000. Is counterion delocalization responsible for collapse in RNA folding? *Biochemistry.* 39:14365–14370.

Nguyen, J. T., H. Inouye, M. A. Baldwin, R. J. Fletterick, F. E. Cohen, S. B. Prusiner, and D. A. Kirschner. 1995. X-ray diffraction of scrapie prion rods and PrP peptides. *J. Mol. Biol.* 252:412–422.

Oldenbourg, R., and W. C. Phillips. 1986. Small permanent magnet for fields up to 2.6 T. *Rev. Sci. Instr.* 57:2362–2365.

Pauling, L., and R. B. Corey. 1953. Compound helical configurations of polypeptide chains: Structure of proteins of the alpha-keratin type. *Nature (Lond.).* 171:59–61.

Richardson, J. S., and D. C. Richardson. 1989. The de novo design of protein structures. *Trends Biochem. Sci.* 14:304–309.

Shirahama, T., and A. S. Cohen. 1967. High-resolution electron microscopic analysis of the amyloid fibril. *J. Cell Biol.* 33:679–708.

Sunde, M., L. C. Serpell, M. Bartlam, P. E. Fraser, M. B. Pepys, and C. C. F. Blake. 1997. Common core structure of amyloid fibrils by synchrotron x-ray diffraction. *J. Mol. Biol.* 273:729–739.

Tanaka, S., and S. Naya. 1969. A theory of x-ray scattering by disordered polymer crystals. *J. Phys. Soc. Japan.* 26:982–993.

Yan, Y. B., A. Tropsha, J. Hermans, and B. W. Erickson. 1993. Free energies for refolding of the common β turn into the inverse-common β turn: Simulation of the role of D/L chirality. *Proc. Natl. Acad. Sci. U.S.A.* 90:7898–7902.

Yan, Y. B., B. W. Erickson, and A. Tropsha. 1995. Free energies for folding and refolding of four types of β turns: Simulation of the role of D/L chirality. *J. Am. Chem. Soc.* 117:7592–7599.